Iron-Binding Process in the Amino- and Carboxyl-Terminal Lobes of Ovotransferrin: Quantitative Studies Utilizing Single Fe^{3+}-Binding Mutants

Ikuko Okamoto, Kimihiko Mizutani, and Masaaki Hirose*

Division of Applied Life Sciences, The Graduate School of Agriculture, Kyoto University, Uji, Kyoto 611-0011, Japan

Received April 28, 2004; Revised Manuscript Received June 30, 2004

ABSTRACT: Iron-liganding-residue mutants of ovotransferrin, Y191F and Y524F, were investigated for their Fe^{3+}-binding properties. The absorption spectrum and urea gel electrophoresis verified the single iron binding on the C- and N-lobes for Y191F and Y524F, respectively. A newly developed competitive Fe^{3+}-binding analysis, in which equimolar Y191F and Y524F are mixed with less Fe^{3+} than saturation, enabled us to quantitatively determine the lobe preference for initial iron entry as the ratio (α value) of N-lobe over C-lobe. The α value estimated on the basis of a kinetic model was highly dependent on pH; within a pH range from 6.5 to 9.0, α was increased from 2 to 5 on lowering pH with an apparent sigmoid curve. On differential scanning calorimetry, single thermal transition was observed around 61 °C for the apo forms of Y191F, Y524F, and wild-type ovotransferrin. The Fe^{3+}-loaded mutants, however, showed dual transitions at 62.4 and 82.1 °C in Y191F and 66.4 and 76.0 °C in Y524F. According to the ΔG_{AB} value that is defined as the free energy change in a target lobe induced by the iron binding on the counter lobe, marked stabilization effects by interlobe interactions were found to be induced during the major iron-binding process: upon the primary N-lobe iron binding in the iron-free C-lobe (ΔG_{AB}, −2.25 kcal/mol) and upon the secondary C-lobe iron binding in the monoferric N-lobe (ΔG_{AB}, −6.45 kcal/mol).

A major egg white protein, oTf,[1] is a member of the transferrin family of iron-binding proteins that includes serum transferrin, lactoferrin, and melanotransferrin (*1*, *2*). Transferrins serve to control the levels of iron in the body fluids of vertebrates by their ability to bind very tightly two Fe^{3+} ions together with two CO_3^{2-} ions. Serum transferrin can act as the iron transporter, while lactoferrin possesses a variety of biological functions, including an antimicrobial activity (*3*) and a sequence-specific DNA-binding capacity (*4*). oTf should share the same structural characteristics as hen serum transferrin, since these proteins are derived from the same gene and they differ only in their attached carbohydrate (*5*). The recent crystal structure of hen serum transferrin (*6*) shows an almost indistinguishable main chain conformation from that of hen oTf (*7*). The existence of the dilysine trigger in the N-lobe is also a common structural characteristic for oTf and serum transferrin (*8*, *9*). Although an iron transport function for oTf for the developing chick embryo has not been proved, specific transferrin−receptor interactions have been demonstrated for egg white oTf (*10*−*12*).

The ∼80 kDa transferrin molecule consists of two homologous N- and C-lobes, which are further divided into two similarly sized domains (N1 and N2 in the N-lobe; C1 and C2 in the C-lobe). The two iron-binding sites are located within the interdomain cleft of each lobe. The two domains of each lobe are closed over an Fe^{3+} ion. Four of the six Fe^{3+} coordination sites are occupied by protein ligands (two Tyr residues, one Asp, and one His) and the other two by a bidentate carbonate anion (*2*).

The transferrin-dependent Fe^{3+} delivery to the target cells occurs in such a way that the diferric transferrin first binds with the specific receptor that resides on the plasma membrane (*13*). The transferrin−receptor complex is then internalized into the cell, and the complex releases Fe^{3+} at acidic pH in the endosome (*13*, *14*). According to the direct comparison of the crystallographic structures of the holo (*7*, *8*, *15*, *16*) and apo (*17*−*20*) forms of oTf, both lobes assume more open domain conformation in the iron-free form than in the diferric form (*21*). Such an iron-dependent conformational change may be closely related to the cellular uptake mechanism of iron; the iron-loaded diferric form shows a higher affinity for the transferrin receptor than does the apo form (*10*, *22*). Despite the equivalent iron coordination structure, the two transferrin lobes behave differently upon the binding and release of iron; there is a lobe preference for the initial entry of iron (*23*−*25*), and the rate for the anion-mediated iron release is much slower from the C-lobe than from the N-lobe (*20*, *26*−*29*). Much increased iron-binding stability at acidic pH of the C-lobe compared with the N-lobe is also a marked lobe difference (*30*). Furthermore, there are complex interlobe interactions that depend on a variety of factors, including the differential extents of iron uptake (*24*, *25*, *31*). Quantitative studies of the iron binding and interlobe interaction in the two lobes are therefore crucial for the understanding of the functional process in the whole molecule of transferrin.

In the present study, single iron-binding oTf mutants, Y191F and Y524F, were produced using a *Pichia pastoris*

* Corresponding author. Phone: +81-774-38-3734. Fax: +81-774-38-3735. E-mail: hirose@kais.kyoto-u.ac.jp.

[1] Abbreviations: oTf, ovotransferrin; FeN-oTf, ovotransferrin with iron-loaded N-lobe; FeC-oTf, ovotransferrin with iron-loaded C-lobe; PAGE, polyacrylamide gel electrophoresis.

10.1021/bi049147j CCC: $27.50
Published on Web 08/06/2004

system and analyzed quantitatively for the lobe preference of the initial iron binding and for the thermal stability of different iron-loaded forms. Here we report a newly developed competitive Fe^{3+}-binding procedure for the analysis of the lobe preference of the initial iron binding. The determined preference factor (α value) is highly dependent on the pH conditions, but at any pH the Fe^{3+}-binding preference is found for the N-lobe. According to the thermal denaturation data, marked stabilization effects by lobe interactions are induced during the major iron-binding process: primarily upon the N-lobe iron binding in the iron-free C-lobe and secondly upon the C-lobe iron binding in the monoferric N-lobe.

EXPERIMENTAL PROCEDURES

Reagents and Preparation of oTf. All of the chemicals were guaranteed grade from Wako Pure Chemical Industries (Osaka, Japan), Nacalai Tesque (Kyoto, Japan) and Sigma-Aldrich Chemicals (St. Louis, MO). Recombinant, wild-type oTf was obtained by a previously established expression procedure using *P. pastoris* (*32*). The oTf mutants of Y191F and Y524F were prepared in the same way except for the inclusion of a site-directed mutagenesis step. A gene encoding oTf and its secretion signal was amplified on pUC18/oTf, ligated into the *P. pastoris* expression vector pPIC3.5 (Invitrogen, Carlsbad, CA), transformed into *Escherichia coli* JM109 strain, and purified as the constructed plasmid, pPIC3.5/oTf, as described (*32*). Mutations of Tyr191 and Tyr524 to phenylalanine were carried out by using a PCR-based mutagenesis procedure (QuikChange mutagenesis kit; Stratagene, La Jolla, CA). The following synthetic oligonucleotides were used to introduce the mutations: Y191F-(+), 5′ GCA CCT TAT TCT GGA TTT TCT GGA GCT TTC C; Y191F(−), 5′ G GAA AGC TCC AGA AAA TCC AGA ATA AGG TGC; Y524F(+), 5′ GAG AAA TAC TTT GGA TTT ACC GGA GCT TTA CGG; and Y524F(−), 5′ CCG TAA AGC TCC GGT AAA TCC AAA GTA TTT CTC (changed nucleotides are underlined). The sequences of the mutant plasmids, pPIC3.5/oTf-Y191F and pPIC3.5/oTf-Y524F, were confirmed using a DNA sequencer (ABI PRISM 310; Applied Biosystems, Foster City, CA). The plasmids were transformed into *P. pastoris*, and oTf mutants Y191F and Y524F were expressed and purified as described (*32*). To prepare the iron-free apo forms, the proteins were incubated in 0.1 M sodium citrate buffer, pH 4.7, and passed through a Sephadex G-25 column (NAP column; Amersham Biosciences, Piscataway, NJ) equilibrated with the same buffer. This procedure was repeated twice, and then the buffer of the protein samples was replaced by 50 mM Tris-HCl, pH 8.0, using the Sephadex column.

N-Terminal Sequence Analysis. The purified recombinant proteins were blotted onto poly(vinylidene fluoride) membrane, and the N-terminal sequences were determined using a protein sequenater (Procise 492; Applied Biosystems, Foster City, CA).

Mass Spectrometry. Protein samples were mixed with 3,5-dimethoxy-4-hydroxycinnamic acid (sinapinic acid) and subjected to matrix-assisted laser desorption/ionization time-of-flight mass spectrometry (Voyager; Applied Biosystems). Bovine serum albumin (Sigma-Aldrich) was used for calibration of molecular weight.

Far-UV CD Spectra. The far-UV circular dichroism (CD) spectra of the iron-loaded forms of oTf were recorded at 0.05 mg/mL in 50 mM Tris-HCl buffer, pH 8.0 and 25 °C, using a spectropolarimeter (model J-720; Jasco, Tokyo, Japan) and a 0.2 cm cuvette.

Analysis for the Iron-Binding Capacity. The iron-free forms of recombinant oTf were titrated at 3.0 mg/mL with increased concentrations of the Fe^{3+}−nitrilotriacetate complex in 50 mM Tris-HCl, pH 8.0, containing 25 mM $NaHCO_3$. Visible absorption spectra were measured at 25 °C using a spectrometer (Ultrospec 2000; Amersham Biosciences), and the iron-binding level was estimated by absorbance at 465 nm. The iron-binding capacity was also analyzed by urea−PAGE (*33*) with minor modification. The proteins were mixed at 1.29 mg/mL with different amounts of the nitrilotriacetate−Fe^{3+} complex in 0.1 M HEPES, pH 7.5, containing 25 mM bicarbonate and incubated overnight at 4 °C. The samples containing 3 μg of proteins were loaded onto a 6.4% polyacrylamide slab gel (89 mm × 68 mm × 1 mm) with a buffer system of 0.1 M Tris−borate, pH 8.4, containing 5.0 M urea and electrophoresed at 150 V for 6 h in a cold room. The gel was then stained with 0.25% Coomassie Brilliant Blue R-250.

Competitive Iron-Binding Analysis. An equimolar mixture of Y191F and Y524F (8.3 μM each) was incubated at 4 °C for 12 h in 0.1 M Na-HEPES (pH 6.5−8.5) or in 0.1 M Tris-HCl (pH 9.0) that contained 25 mM $NaHCO_3$ and different concentrations of the Fe^{3+}−nitrilotriacetate complex. The samples were analyzed for their iron binding by urea−PAGE in the same way. The protein bands were quantified with the software SCION image (version Beta 4.0.2; Scion Corp., Frederick, MD).

Differential Scanning Calorimetry. As in the protocol shown for egg white oTf (*25*), the thermal stabilities of the recombinant proteins were analyzed in 0.5 M HEPES, pH 7.5, containing 25 mM $NaHCO_3$ with a differential scanning calorimeter (MCS-DSC; Micro Cal, Northampton, MA). For analysis of the iron-loaded Y191F and Y524F, the proteins were mixed, prior to the calorimetric analysis, with the Fe^{3+}−nitrilotriacetate complex at an iron to protein molar ratio of 2.0 in the same buffer and incubated overnight at 4 °C. The recombinant wild-type protein was mixed with the Fe^{3+}−nitrilotriacetate complex at different iron to protein ratios and incubated in the same way. The protein concentration was 0.4 mg/mL, and the rate of temperature change was 1 °C/min. The enthalpy change ΔH_m at the transition temperature and the heat capacity change ΔC_p for the transition were calculated as described (*25*); two-state transition was assumed for the curve-fitting analysis for ΔC_p, and ΔH_m was obtained by area integration of the endothermic peak using the software Origin (Micro Cal).

RESULTS

Structural Characteristics of oTf Mutants. Wild-type recombinant oTf is totally secreted into the culture medium from *P. pastoris* cells (*32*). The same was also true for oTf mutants Y191F and Y524F. The N-terminal sequence of the purified oTf mutants was analyzed with a sequenator and determined to be Ala-Pro-Pro-Lys- for Y191F and Y524F; the sequence was consistent with the N-terminal sequence of egg white oTf. The expression vector included the

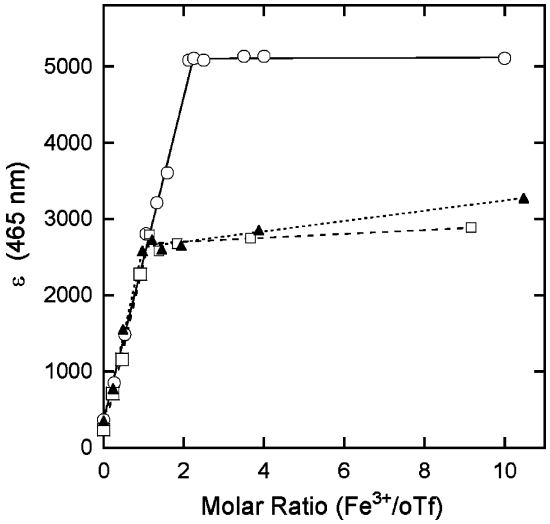

FIGURE 1: Fe^{3+}-binding capacities of oTf. Recombinant wild-type oTf (open circles), Y191F (closed triangles), and Y524F (open squares) were incubated at various molar ratios of the Fe^{3+}−nitrilotriacetate complex to protein in 50 mM Tris-HCl, pH 8.0, containing 25 mM $NaHCO_3$. Visible absorption spectra were measured at 25 °C, and the iron-binding level was estimated by absorbance at 465 nm.

N-terminal signal sequence of the egg white protein. The signal sequence was, therefore, concluded to be correctly processed during the secretion from *P. pastoris* cells.

The molecular weights determined by matrix-assisted laser desorption/ionization time-of-flight mass spectrometry were 77943 and 77835 for Y191F and Y524F, respectively. These values were significantly greater than the theoretical value (75836) for the polypeptide entity. A similar greater value has previously been found for the wild-type oTf, expressed in the same *P. pastoris* system; the observed molecular weight is 77801, while the theoretical polypeptide value is 75852 (*32*). For the wild-type oTf, the increased molecular weight has been accounted for by the attached high-mannose carbohydrate chain, since the protein displayed, after cleavage by endo-*β*-*N*-acetylglucosaminidase, almost the same molecular weight of 75925 as the theoretical value (polypeptide plus putative core glycosylation by *N*-acetylglucosamine: 76055). It is therefore very likely that the increased molecular weights for the oTf mutants come from the attached carbohydrate chain.

The far-UV CD spectra of oTf mutants Y191F and Y524F were almost indistinguishable from that of egg-white oTf (data not shown), which indicates essentially the same secondary structure contents for these proteins.

Iron-Binding Capacity. The visible absorption spectra for the iron-loaded forms of Y191F and Y524F showed the same intensity at a λ_{max} of 465 nm (data not shown). To perform stoichiometric analyses for the iron binding, Y191F, Y524F, and wild-type oTf were titrated with the Fe^{3+}−nitrilotriacetate complex, and the intensities of absorbance at 465 nm were determined. As shown in Figure 1, the titrations of Y191F and Y524F were both saturated at an iron to protein ratio of 1:1, while the saturation was achieved at a 2:1 ratio with respect to wild-type oTf. In addition, the absorbance intensity at the iron saturation was almost exactly twice that for the wild-type protein as compared to the mutant proteins. These data demonstrate the existence of a single iron-binding site for eitherY191F or Y524F.

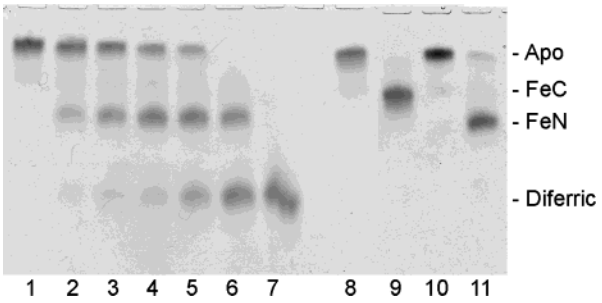

FIGURE 2: Urea−PAGE analysis. Recombinant wild-type oTf (lanes 1−7) was incubated at different iron to protein molar ratios (Fe^{3+}−nitrilotriacetate complex/oTf: lane 1, 0; lane 2, 0.25; lane 3, 0.5; lane 4, 0.75; lane 5, 1.0; lane 6, 1.5; lane 7, 2.0) and analyzed by urea−PAGE as described in the text. For the analyses of oTf mutants, Y191F (lanes 8 and 9) and Y524F (lanes 10 and 11) were incubated in the presence (lanes 9 and 11) and absence (lanes 8 and 10) of a 20 times molar excess of Fe^{3+}−nitrilotriacetate and analyzed by urea−PAGE in the same way.

The iron-binding capacity was also analyzed by urea−PAGE. Urea-denaturing conditions can be optimized for transferrins, so that the iron-free lobes are fully denatured with extended conformation without any denaturation of the iron-loaded lobes (*33*). The extent of conformational extension and electrostatic situations in the denatured state should not be identical for the two lobes, because of different numbers of intrachain disulfides and of different amino acid compositions. These enable us to distinctly separate apo oTf, diferric oTf, FeN-oTf, and FeC-oTf by PAGE in the presence of urea. For monoferric oTf, the protein bands with lower and higher mobilities have been assigned as FeC-oTf and FeN-oTf, respectively (*33*). Figure 2 shows that all of the three iron-loaded oTf forms can be detected for wild-type oTf during the iron saturation. For a mutant protein, however, only a single iron-loaded band was detected: an FeC-oTf band for Y191F and an FeN-oTf band for Y524F. We therefore concluded that Y191F and Y524F have a single iron-binding site on the C- and N-lobes, respectively.

Competitive Iron-Binding Analysis. Previous reports have shown the preference of the N-lobe for the initial entry of iron in egg white oTf, although it is not so strong as the preference for the C-lobe in human serum transferrin (*23*, *25*). Figure 2 shows that this is indeed the case also for the recombinant wild-type oTf. The occurrence in the wild-type protein of a second iron binding to FeN-oTf and/or to FeC-oTf even at a low iron level makes it difficult to directly determine the extent of the lobe preference. We therefore employed a novel approach to determine the lobe preference for the initial iron binding utilizing the single iron-binding mutants. In this approach, an equimolar amount of Y191F and Y524F was mixed with a less molar amount of Fe^{3+} than saturation, and after competitive iron binding the relative level of FeN-oTf and FeC-oTf was determined.

The relative iron-binding capacity of the two lobes was analyzed by urea−PAGE after competitive iron binding of equimolar Y191F and Y524F. Figure 3A shows the electrophoretic profiles of the mixed oTf mutants after the iron binding at pH 7.0. When the added iron was increased, the band intensity of apo oTf decreased and the monoferric band intensities of FeN-oTf and FeC-oTf increased. The band intensities were quantified and plotted as a function of the saturation levels of iron. As shown in Figure 3B, the

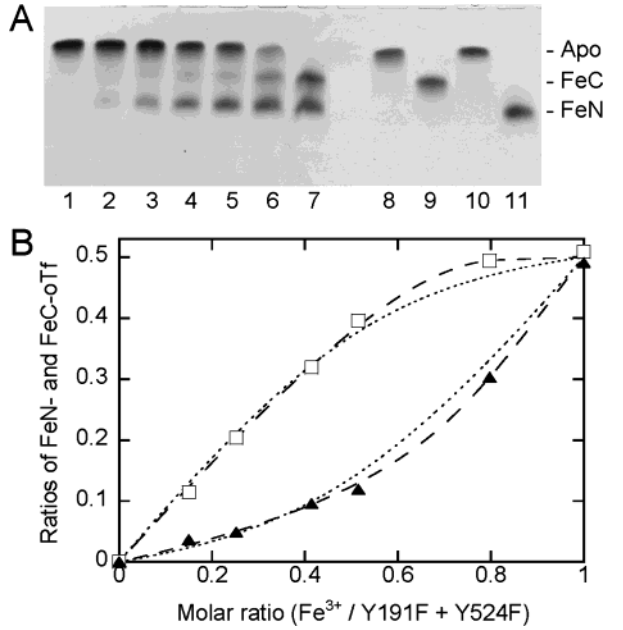

FIGURE 3: Competitive iron-binding analysis. (A) An equimolar mixture of Y191F and Y524F (8.3 μM each) was incubated at different iron to protein molar ratios (Fe^{3+}−nitrilotriacetate/Y191F + Y524F: lane 1, 0; lane 2, 0.15; lane 3, 0.25; lane 4, 0.41; lane 5, 0.52; lane 6, 0.80; lane 7, 1.0) for 12 h in 0.1 M Na-HEPES (pH 7.0) containing 25 mM $NaHCO_3$. The samples were analyzed by urea−PAGE. (B) The protein bands were quantified for apo-oTf, FeN-oTf, and FeC-oTf. The ratios of the band intensities of FeN-oTf (R_N, open squares) and FeC-oTf (R_C, closed triangles), relative to the total intensity of the three protein bands, were analyzed by curve fittings to eqs 5 and 6 for the kinetic model and eqs 11 and 12 for the thermodynamic model described in the text. The slashed and dotted curves are the fitted ones for the kinetic and thermodynamic models, respectively. The obtained α values were 5.0 ± 0.18 (SE) and 4.9 ± 0.31 (SE) on the kinetic model for the analyses of FeN-oTf and FeC-oTf, respectively. The corresponding α values were 8.1 ± 3.6 (SE) and 6.9 ± 1.1 (SE) on the thermodynamic model.

increases in FeN-oTf and FeC-oTf with the progress of iron saturation displayed nonlinear curves; at low iron saturation, the iron-binding level was much greater for the N-lobe than for the C-lobe, which reflects the N-lobe preference of the initial iron binding.

To quantitatively determine the extent of the lobe preference, we employed a curve-fitting analysis for the urea−PAGE data. The iron-binding process includes multiple steps: the binding of the Fe^{3+}−nitrilotriacetate complex to the domain-opened apo form and subsequent domain closure following the replacement of nitrilotriacetate by the carbonate anion (*34*). A quantitative equation that expresses the overall iron-binding process has not been at our hand. We therefore examined both kinetic and thermodynamic models for the lobe preference. For the kinetic model, the Fe^{3+}-binding reactions to the two lobes can be shown as follows:

$$\text{Y524F} + \text{Fe}^{3+} \xrightarrow{k_N} \text{FeN-oTf} \quad (1)$$

$$\text{Y191F} + \text{Fe}^{3+} \xrightarrow{k_C} \text{FeC-oTf} \quad (2)$$

where k_N and k_C represent the second-order rate constants of the binding of Fe^{3+} to the N-lobe and C-lobe, respectively. In the present study, the same molar amount of Y191F and Y524F was incubated with less molar amounts of Fe^{3+} than saturation for a prolonged time that led to the completion of iron binding. The concentration of added Fe^{3+} ($[Fe^{3+}]_{total}$), therefore, should correspond to the sum of the concentrations of Fe^{3+}-bound Y191F and Y524F:

$$[\text{Fe}^{3+}]_{total} = [\text{FeN-oTf}] + [\text{FeC-oTf}] \quad (3)$$

On the molar ratio basis, the equation is expressed by

$$R_T = R_N + R_C \quad (4)$$

where R_T, R_N, and R_C are respectively the molar ratios of $[Fe^{3+}]_{total}$, [FeN-oTf], and [FeC-oTf], relative to the sum of the concentrations of Y191F and Y524F. When α is defined as the ratio of k_N to k_C ($\alpha = k_N/k_C$), the equations in which R_T is related to each of R_N and R_C are obtained by integration of the differential equations derived from eqs 1 and 2:

$$R_T = 0.5 + R_C - [0.5(0.5 - R_C)^{\alpha}]/(0.5)^{\alpha} \quad (5)$$

$$R_T = 0.5 + R_N - [0.5(0.5 - R_N)^{1/\alpha}]/(0.5)^{1/\alpha} \quad (6)$$

In the thermodynamic model, the two lobes compete for iron binding in the equilibrium state:

$$\text{Y524F} + \text{Fe}^{3+} \overset{K_{bN}}{\rightleftharpoons} \text{FeN-oTf} \quad (7)$$

$$\text{Y191F} + \text{Fe}^{3+} \overset{K_{bC}}{\rightleftharpoons} \text{FeC-oTf} \quad (8)$$

where K_{bN} and K_{bC} are the binding constants of iron to each lobe.

$$K_{bN} = [\text{FeN-oTf}]/[\text{Fe}^{3+}][\text{Y524F}] \quad (9)$$

$$K_{bC} = [\text{FeC-oTf}]/[\text{Fe}^{3+}][\text{Y191F}] \quad (10)$$

When α is defined as the ratio of K_{bN} to K_{bC} ($\alpha = K_{bN}/K_{bC}$), R_T is related to R_N and R_C as follows:

$$R_T = R_C(0.5 + 0.5\alpha - R_C + \alpha R_C)/(0.5 - R_C + \alpha R_C) \quad (11)$$

$$R_T = R_N(0.5 + 0.5\alpha - \alpha R_N + R_N)/(0.5\alpha - \alpha R_N + R_N) \quad (12)$$

Figure 3B demonstrates the fitting curves of the iron-binding data utilizing eqs 5 and 6 for the kinetic model and eqs 11 and 12 for the thermodynamic model. The curve fittings by the kinetic model showed less errors and much better agreement between the FeN-oTf and FeC-oTf analyses than those by the thermodynamic model; the estimated α values for the kinetic model were 5.0 ± 0.18 (SE) and 4.9 ± 0.31 (SE) for the FeN-oTf and FeC-oTf analyses, respectively, while corresponding values were 8.1 ± 3.6 (SE) and 6.9 ± 1.1 (SE) for the thermodynamic model. These data demonstrate that the kinetic model practically works more precisely for the lobe preference analysis than the thermodynamic model.

The competitive iron-binding experiment was done at various pH values, and the α value was estimated by the curve-fitting analysis on the basis of the kinetic model. Figure 4 displays α values as a function of pH. The α value showed marked pH dependence with increased values on lowering

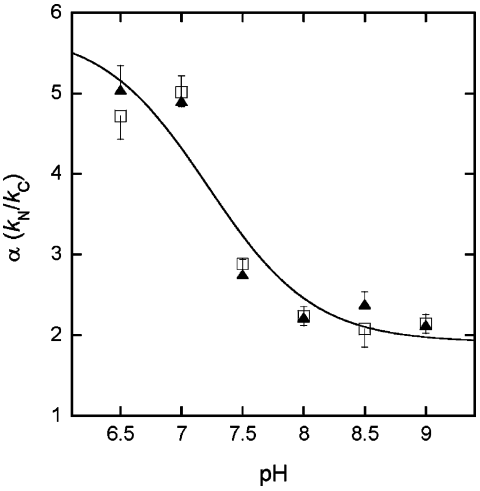

FIGURE 4: Effects of pH on the lobe preference for the initial entry of iron. An equimolar mixture of Y191F and Y524F was incubated at various pH with different concentrations of Fe^{3+}−nitrilotriacetate and analyzed by urea−PAGE in the same way as in Figure 3. The obtained α values on the basis of the kinetic model for FeN-oTf (open squares) and FeC-oTf (closed triangles) were plotted as a function of pH. The error bars (downward for the FeN-oTf analyses and upward for the FeC-oTf analyses) represent the standard errors (SE) on the curve-fitting analyses. The solid curve represents the fitted one for the α values to the equation $pH = pK_a + \log[(\alpha_{max} - \alpha)/(\alpha - \alpha_{min})]$, where α_{max} and α_{min} are the theoretical maximum and minimum values of α, respectively. In this equation, the involvement in the lobe preference of protonation of (an) amino acid residue(s) with a single class of pK_a is hypothesized. In this hypothesis, the obtained pK_a was 7.2.

pH. The pH dependence profile was consistent with a sigmoid curve, derived from a hypothesis that the protonation of (an) amino acid residue(s) with a single class of pK_a value is involved in the control of the lobe preference. In this hypothesis, the pK_a value obtained by the curve fitting was 7.2 with the maximum and minimum α values of 6.0 and 1.9, respectively.

Interlobe Interactions Analyzed by Differential Scanning Calorimetry. Previous calorimetric studies of egg white oTf have revealed the presence of four endothermic peaks in a partially iron-saturated condition (*25*, *35*). To obtain an unequivocal conclusion for the assignment of endothermic peaks, we did differential scanning calorimetric analyses for the iron-loaded and iron-free forms of recombinant wild-type and mutant oTf. As shown in Figure 5A, the endothermic profiles of recombinant wild-type oTf were essentially the same as the previous data of nonrecombinant egg white oTf (*25*) during the progress of iron saturation; the observed endothermic peaks were at 61, 65, 76, and 82 °C. The lowest and highest peaks correspond to the ones by the thermal transitions of the iron-free apo and diferric holo forms, respectively.

The two intermediate endothermic peaks were clearly assigned by the analyses of Y191F and Y524F. As shown in Figure 5B, the iron-free apo forms of Y191F and Y524F displayed a single thermal transition around 61 °C. The Fe^{3+}-loaded forms of these oTf mutants, however, showed dual thermal transition profiles. The detected denaturation temperatures were 62.4 and 82.1 °C for Y191F and 66.4 and 76.0 °C for Y524F. The data clearly confirm that the two intermediate endothermic peaks for wild-type oTf come from the denaturation of the two lobes of a single monoferric species of FeN-oTf; the endothermic transitions at 66.4 and 76.0 °C should correspond to the denaturation of the iron-free N-lobe and that of the iron-loaded C-lobe, respectively. It was also found that the peaks for iron-loaded Y191F (FeC-oTf) correspond to the denaturation of the iron-free N-lobe (62.4 °C) and that of the iron-loaded C-lobe (82.1 °C). The lower and higher transition temperatures for FeC-oTf were almost the same as those for iron-free apo and diferric holo forms of wild-type oTf, respectively.

Table 1 summarizes the thermodynamic values for the thermal denaturation in the two lobes of oTf mutants. The terms T_m and T_m' represent respectively the thermal denaturation temperature of a target lobe before and after iron binding in the counter lobe. The value ΔG_{AB} that is the measure for the free energy change in a target lobe induced

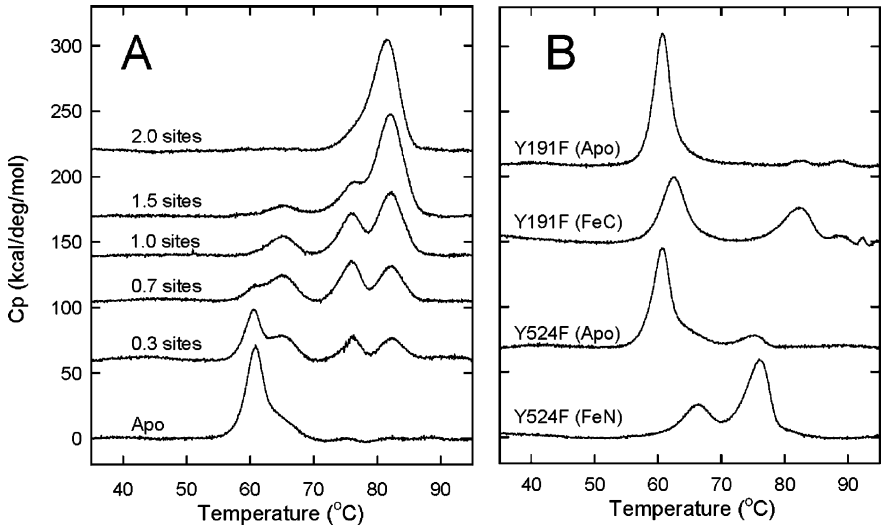

FIGURE 5: Thermal transition profiles of recombinant wild-type and mutant oTf. In panel A, the recombinant wild-type oTf was mixed with the Fe^{3+}−nitrilotriacetate complex at different iron to protein ratios in 0.5 M HEPES, pH 7.5, containing 25 mM $NaHCO_3$. After incubation overnight at 4 °C, the protein was analyzed with a differential scanning calorimeter as described in the text. In panel B, Y191F and Y524F were incubated overnight at 4 °C in 0.5 M HEPES, pH 7.5, containing 25 mM $NaHCO_3$ in the presence (FeC-oTf and FeN-oTf) and absence (apo) of Fe^{3+}−nitrilotriacetate at an iron to protein molar ratio of 2.0 and analyzed by differential scanning calorimetry in the same way.

Table 1: Thermodynamic Constants[a]

target lobe	T_m (°C)	T_m' (°C)	ΔH_m (kcal/mol)	$\Delta H_m'$ (kcal/mol)	ΔG_{AB} (kcal/mol)	oTf
iron-free N	61.5	62.4	231[c]	237[b]	−0.63	Y191F
iron-free C	61.7	66.4	145[c]	175[b]	−2.25	Y524F
iron-loaded N	76.0	81.8[d]	368[b]		−6.46	Y524F
iron-loaded C	82.1	81.8[d]	150[b]		0.14	Y191F

[a] T_m and ΔH_m represent respectively the thermal transition temperature and the enthalpy change upon the denaturation of a target lobe, when the counter lobe is in the iron-free state. T_m' and $\Delta H_m'$ are the corresponding values for a target lobe, when the counter lobe is loaded with iron. The heat capacity change ΔC_p for the transition was estimated as the half value of the bilobal data obtained for the apo form of mutant oTf (Figure 5); it was 6.40 kcal mol^{-1} deg^{-1} for Y524F and 7.10 kcal mol^{-1} deg^{-1} for Y191F. Using the T_m, T_m', ΔH_m, and ΔC_p values, ΔG_{AB}, which is defined as the free energy change in a target lobe induced by iron binding in the counter lobe, was calculated using eq 13 as described in the text. [b] The values obtained from the peak areas of the differential scanning calorimetry analysis (Figure 5). [c] The values obtained by calculation using the equation $\Delta H_m = \Delta H_m' + \Delta C_p(T_m - T_m')$. [d] The transition temperature of the diferric wild-type oTf.

by iron binding on the counter lobe is defined as follows (*25*):

$$\Delta G_{AB}(T_m') = \Delta H_m[1 - (T_m'/T_m)] + \Delta C_p[T_m' \ln(T_m/T_m') + T_m' - T_m] \quad (13)$$

According to the ΔG_{AB} values, strong stabilization effects were concluded to be induced in the iron-free C-lobe by the N-lobe iron binding (−2.25 kcal/mol) and in the monoferric N-lobe by the C-lobe iron binding (−6.46 kcal/mol). The free energy change in the iron-free N-lobe upon the C-lobe iron binding was very small with ΔG_{AB} of −0.63 kcal/mol. More strikingly, the thermodynamic effect in the monoferric C-lobe upon the N-lobe iron binding was almost absent or even destabilizing (ΔG_{AB}, 0.14 kcal/mol).

DISCUSSION

As a common structural characteristic for all of the transferrin lobes, four of the six Fe^{3+} coordination sites are occupied by protein ligands and the other two by a bidentate carbonate anion; the protein ligands are the side chains of one Asp residue (D60 in the oTf N-lobe or D395 in the oTf C-lobe), two Tyr residues (Y92 and Y191 in the oTf N-lobe or Y431 and Y524 in the oTf C-lobe), and one His residue (H250 in the oTf N-lobe or H592 in the oTf C-lobe) (*2*, *21*). Previous mutagenesis studies have shown that the replacements of the coordinating Asp and His residues by different amino acid residues do not completely abolish the iron-binding nature (*36*−*39*). In contrast, the double mutation of the two Tyr residues leads to complete loss of iron-binding capacity in either lobe (*31*). The data of the current study clearly demonstrate that the mutagenesis of a coordinating Tyr residue of Y191 or of Y524 leads to the complete loss of the iron-binding capacity in either lobe (Figures 1 and 2). Likewise, the equivalent tyrosine residue of Y191 in the N-terminal half-molecule of human serum transferrin (Y188) has been shown to be essential for iron binding (*40*). Residues Y191 and Y524 are the only protein ligands that come from domain 2 (domains N2 and C2, respectively) (*7*, *8*, *15*, *16*). Furthermore, these Tyr residues play a central role for the primary iron binding on the domain-opened transferrin form

Scheme 1[a]

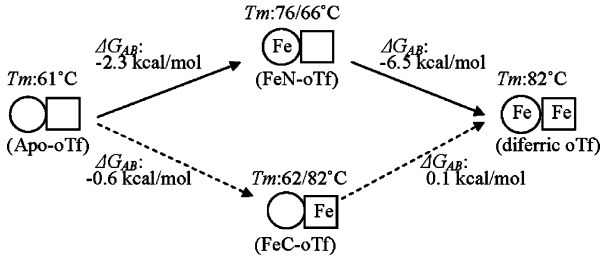

[a] The circles and squares show the N-lobe and C-lobe, respectively; they include "Fe" when the corresponding lobes are loaded with iron. The solid and slashed arrows represent the major and minor iron uptake processes, respectively. T_m and ΔG_{AB} are shown as approximated values.

(*34*, *41*). These are probably the reason the replacement of Y191 and Y524 by a noncoordinating Phe residue results in a complete loss of iron-binding capacity.

Analyses of the interlobe interactions utilizing single iron-binding mutants have previously been done with lactoferrin (*31*), which has a unique property to retain iron at lower pH values than other transferrins. The results have clearly demonstrated the presence of cooperative interactions between the two iron-loaded lobes at acidic pH: diferric wild-type lactoferrin retains both of the iron atoms at an acidic pH value in which the N-lobe monoferric mutant completely loses the loaded iron. In the current study, we employed iron-binding mutants by alternative ways for the analysis of iron-binding characteristics of the two lobes. The obtained data can be summarized as shown in Scheme 1.

Previous reports have shown the preference of the N-lobe for the initial entry of iron in egg white oTf, although it is not so absolute as the preference for the C-lobe in human serum transferrin (*23*, *25*). This was indeed the case also for the recombinant wild-type oTf (Figure 2). The occurrence in the wild-type protein of a second iron binding to FeN-oTf and/or to FeC-oTf even at a low level of iron makes it difficult to quantitatively determine the extent of the lobe preference. In the current study, we newly employed a competitive binding approach to determine the lobe preference utilizing single iron-binding mutants. In this analysis, the intramolecular iron-binding competition of the two lobes is designed to be replaced by the bimolecular lobe competition, thereby making possible the clear determination of the lobe preference for the initial entry of iron. The obtained data demonstrate the N-lobe preference, but the preference is not absolute (Figure 3). Furthermore, the preference factor (α value) of the N-lobe over the C-lobe significantly depends on pH values; the preference for the N-lobe increased with lowering pH. The pH dependence profile was consistent with a sigmoid curve, derived from a hypothesis that the protonation of (a) amino acid residue(s) with a single class of pK_a value of about pH 7 is involved in the control of the lobe preference (Figure 4). The observed pK_a value suggests the participation of (a) histidine residue(s) of oTf as a determinant of the lobe preference.

The lobe preference for the initial entry of Fe^{3+} is also variable depending on the added iron form and on transferrin species. In the current study, the Fe^{3+}−nitrilotriacetate complex was added to recombinant oTf. When the nitrilotriacetate complex is substituted for by $FeCl_3$ in the presence of $NaHCO_3$, the N-lobe preference is abolished in egg white oTf (*23*). In human serum transferrin, the lobe preference

of the added Fe^{3+}−nitrilotriacetate complex is almost absolute for the C-lobe (*25*, *42*), while the N-lobe preference is detected upon the addition of the Fe^{3+}−citrate complex (*42*). The detailed mechanism underlying the lobe preference which depends on the anionic ligand bound to iron is not clear at present. The current competitive iron-binding method should provide a crucial tool for the better understanding of the mechanism.

By calorimetric studies of egg white oTf, the presence of four endothermic peaks has been detected in a partially iron-saturated condition (*25*, *35*). The endothermic transitions with the lowest (60−63 °C) and highest transition temperatures (82−84 °C) have been assigned as those of the iron-free apo and diferric holo forms, respectively. With respect to the molecular assignment for the two intermediate endothermic peaks (66−68 and 76−77 °C), however, there has been disagreement as to whether the two thermal transitions come from different molecular species of monoferric forms (FeN-oTf and FeC-oTf) or from different lobes of a single monoferric species of FeN-oTf (*25*, *35*). The former assignment has led the authors to conclude only slight lobe preference for the initial iron binding (*35*). In contrast, the latter assignment depended, as a prerequisite, on the preference for the N-lobe under partially iron-saturated conditions, although the N-lobe preference has been shown to be relative (*23*).

The current differential scanning calorimetric analyses (Figure 5) for Y191F and Y524F provide the unequivocal conclusion for the thermal transitions of two lobes that the intermediate endothermic peaks at 66.4 and 76.0 °C are accounted for by the thermal denaturation of the iron-free C-lobe and the iron-loaded N-lobe, respectively, in a single FeN-oTf molecule. The conclusion that the two endothermic peaks of 62.4 and 82.1 °C for the iron-loaded Y191F (FeC-oTf) come from the denaturation of the iron-free N-lobe and that of the iron-loaded C-lobe, respectively, was also obtained for the first time by the use of the single iron-binding mutant. The lower and higher transition temperatures for FeC-oTf are almost indistinguishable from those for iron-free apo and diferric holo forms of wild-type oTf, respectively. Because of these indistinguishable transition temperatures, the two transition temperatures have not been clearly assigned for FeC-oTf in the previous study using egg white oTf (*25*).

About the cooperative interactions between the two lobes, the determination of a single ΔG_{AB} value has been possible for egg white oTf; the estimated value is −3.1 kcal/mol for the free energy change of the iron-free C-lobe by the iron binding in the N-lobe (*25*). The current thermodynamic values were more directly determined using the oTf mutants (Table 1). The estimated ΔG_{AB} value for the same cooperative interaction was a smaller absolute value of −2.25 kcal/mol. The disagreement comes, at least in part, from the differential estimate of the ΔH_m value; in the previous report, the ΔH_m value for the C-lobe has been estimated as half of the total endothermic area of the two lobes (*25*), while in the current study, the value was determined directly using Y524F. More importantly, the current use of the oTf mutants extended the quantitative determinations about the cooperative interaction of the two lobes. The newly estimated ΔG_{AB} values were −0.63 and −6.46 kcal/mol, respectively, for the free energy changes of the iron-free and iron-loaded N-lobe by the iron binding in the C-lobe (Table 1). The thermodynamic effect of the N-lobe iron binding on the iron-loaded C-lobe is almost absent or even slightly destabilizing.

The asymmetric interlobe interactions as detected by the differential thermal stabilization may be related to the structural situations of the two lobes of oTf. There are two structural regions for the interactions of the two lobes of oTf. One is the peptide segment consisting of residues 333−341 that connects the two lobes covalently (*7*, *15*, *18*). After removal of this segment by tryptic digestion, however, the isolated two half-molecules are still associated with each other through an alternative class of the lobe interactions in which the C-terminal helix 12 (residues 674−686 in the C-lobe) plays a central role (*43*−*45*). Helix 12 exists in the C-lobe alone and undergoes strong noncovalent interactions with an interdomain hinge of the N-lobe (*18*) that plays a central role for the domain motion in the N-lobe upon iron uptake and release (*16*). Helix 12 includes Cys680 that makes a disulfide bond with Cys405 in the C-lobe; Asp395, an Fe^{3+} ligand in the C-lobe, is located at the N-terminus of helix 3 (residues 395−405) while Cys405 is at the C-terminus of this helix (*7*, *15*, *18*). The functionally important hinge residues in the N-lobe and the iron ligating residues of Asp395 in the C-lobe are therefore involved in an interlobe interaction network formed by a central participation of helix 12 (*18*). These asymmetric structural properties of the two lobes are probably related to the differential modes of the interlobe communications.

REFERENCES

1. Aisen, P., and Listowsky, I. (1980) Iron transport and storage proteins, *Annu. Rev. Biochem. 49*, 357−393.
2. Baker, H. M., Anderson, B. F., and Baker, E. N. (2003) Dealing with iron: common structural principles in proteins that transport iron and heme, *Proc. Natl. Acad. Sci. U.S.A. 100*, 3579−3583.
3. Arnold, R. R., Cole, M. F., and McGhee, J. R. (1977) A bactericidal effect for human lactoferrin, *Science 197*, 263−265.
4. He, J., and Furmanski, P. (1995) Sequence specificity and transcriptional activation in the binding of lactoferrin to DNA, *Nature 373*, 721−724.
5. Thibodeau, S. N., Lee, D. C., and Palmiter, R. D. (1978) Identical precursors for serum transferrin and egg white conalbumin, *J. Biol. Chem. 253*, 3771−3774.
6. Guha Thakurta, P., Choudhury, D., Dasgupta, R., and Dattagupta, J. K. (2003) Structure of diferric hen serum transferrin at 2.8 Å resolution, *Acta Crystallogr., Sect. D: Biol. Crystallogr. 59*, 1773−1781.
7. Kurokawa, H., Mikami, B., and Hirose, M. (1995) Crystal structure of diferric hen ovotransferrin at 2.4 Å resolution, *J. Mol. Biol. 254*, 196−207.
8. Dewan, J. C., Mikami, B., Hirose, M., and Sacchettini, J. C. (1993) Structural evidence for a pH-sensitive dilysine trigger in the hen ovotransferrin N-lobe: implications for transferrin iron release, *Biochemistry 32*, 11963−11968.
9. MacGillivray, R. T., Moore, S. A., Chen, J., Anderson, B. F., Baker, H., Luo, Y., Bewley, M., Smith, C. A., Murphy, M. E., Wang, Y., Mason, A. B., Woodworth, R. C., Brayer, G. D., and Baker, E. N. (1998) Two high-resolution crystal structures of the recombinant N-lobe of human transferrin reveal a structural change implicated in iron release, *Biochemistry 37*, 7919−7928.
10. Brown-Mason, A., and Woodworth, R. C. (1984) Physiological levels of binding and iron donation by complementary half-molecules of ovotransferrin to transferrin receptors of chick reticulocytes, *J. Biol. Chem. 259*, 1866−1873.
11. Mason, A. B., Brown, S. A., and Church, W. R. (1987) Monoclonal antibodies to either domain of ovotransferrin block binding to transferrin receptors on chick reticulocytes, *J. Biol. Chem. 262*, 9011−9015.
12. Mason, A. B., Woodworth, R. C., Oliver, R. W., Green, B. N., Lin, L. N., Brandts, J. F., Savage, K. J., Tam, B. M., and MacGillivray, R. T. (1996) Association of the two lobes of

ovotransferrin is a prerequisite for receptor recognition. Studies with recombinant ovotransferrins, *Biochem. J. 319*, 361−368.
13. Dautry-Varsat, A., Ciechanover, A., and Lodish, H. F. (1983) pH and the recycling of transferrin during receptor-mediated endocytosis, *Proc. Natl. Acad. Sci. U.S.A. 80*, 2258−2262.
14. Klausner, R. D., Ashwell, G., van Renswoude, J., Harford, J. B., and Bridges, K. R. (1983) Binding of apotransferrin to K562 cells: explanation of the transferrin cycle, *Proc. Natl. Acad. Sci. U.S.A. 80*, 2263−2266.
15. Rawas, A., Muirhead, H., and Williams, J. (1996) Structure of diferric duck ovotransferrin at 2.35 angstrom resolution, *Acta Crystallogr., Sect. D: Biol. Crystallogr. 52*, 631−640.
16. Mizutani, K., Mikami, B., and Hirose, M. (2001) Domain closure mechanism in transferrins: new viewpoints about the hinge structure and motion as deduced from high-resolution crystal structures of ovotransferrin N-lobe, *J. Mol. Biol. 309*, 937−947.
17. Rawas, A., Muirhead, H., and Williams, J. (1997) Structure of apo duck ovotransferrin: The structures of the N and C lobes are in the open form, *Acta Crystallogr., Sect. D: Biol. Crystallogr. 53*, 464−468.
18. Kurokawa, H., Dewan, J. C., Mikami, B., Sacchettini, J. C., and Hirose, M. (1999) Crystal structure of hen apo-ovotransferrin. Both lobes adopt an open conformation upon loss of iron, *J. Biol. Chem. 274*, 28445−28452.
19. Mizutani, K., Yamashita, H., Mikami, B., and Hirose, M. (2000) Crystal structure at 1.9 Å resolution of the apoovotransferrin N-lobe bound by sulfate anions: implications for the domain opening and iron release mechanism, *Biochemistry 39*, 3258−3265.
20. Mizutani, K., Muralidhara, B. K., Yamashita, H., Tabata, S., Mikami, B., and Hirose, M. (2001) Anion-mediated Fe^{3+} release mechanism in ovotransferrin C-lobe: a structurally identified SO_4^{2-} binding site and its implications for the kinetic pathway, *J. Biol. Chem. 276*, 35940−35946.
21. Hirose, M. (2000) The structural mechanism for iron uptake and release by transferrins, *Biosci., Biotechnol., Biochem. 64*, 1328−1336.
22. Young, S. P., Bomford, A., and Williams, R. (1984) The effect of the iron saturation of transferrin on its binding and uptake by rabbit reticulocytes, *Biochem. J. 219*, 505−510.
23. Williams, J., Evans, R. W., and Moreton, K. (1978) The iron-binding properties of hen ovotransferrin, *Biochem. J. 173*, 533−539.
24. Nakazato, K., Yamamura, T., and Satake, K. (1988) Different stability of N- and C-domain of diferric ovotransferrin in urea and application to the determination of iron distribution between the two domains, *J. Biochem. (Tokyo) 103*, 823−828.
25. Lin, L. N., Mason, A. B., Woodworth, R. C., and Brandts, J. F. (1994) Calorimetric studies of serum transferrin and ovotransferrin. Estimates of domain interactions, and study of the kinetic complexities of ferric ion binding, *Biochemistry 33*, 1881−1888.
26. Kretchmar, S. A., and Raymond, K. N. (1986) Biphasic kinetics and temperature-dependence of iron removal from transferrin by 3,4-licams, *J. Am. Chem. Soc. 108*, 6212−6218.
27. Bali, P. K., and Harris, W. R. (1989) Cooperativity and heterogeneity between the 2 binding-sites of diferric transferrin during iron removal by pyrophosphate, *J. Am. Chem. Soc. 111*, 4457−4461.
28. Bali, P. K., Harris, W. R., and Nessettollefson, D. (1991) Kinetics of iron removal from monoferric and cobalt-labeled monoferric human serum transferrin by nitrilotris(methylenephosphonic acid) and nitrilotriacetic acid, *Inorg. Chem. 30*, 502−508.
29. Muralidhara, B. K., and Hirose, M. (2000) Anion-mediated iron release from transferrins. The kinetic and mechanistic model for N-lobe of ovotransferrin, *J. Biol. Chem. 275*, 12463−12469.
30. Mazurier, J., and Spik, G. (1980) Comparative study of the iron-binding properties of human transferrins, *Biochim. Biophys. Acta 629*, 399−408.
31. Ward, P. P., Zhou, X., and Conneely, O. M. (1996) Cooperative interactions between the amino- and carboxyl-terminal lobes contribute to the unique iron-binding stability of lactoferrin, *J. Biol. Chem. 271*, 12790−12794.
32. Mizutani, K., Okamoto, I., Fujita, K., Yamamoto, K., and Hirose, M. (2004) Structural and functional characterization of ovotransferrin produced by *Pichia pastoris*, *Biosci., Biotechnol., Biochem. 68*, 376−383.
33. Evans, R. W., and Williams, J. (1980) The electrophoresis of transferrins in urea/polyacrylamide gels, *Biochem. J. 189*, 541−546.
34. Mizutani, K., Yamashita, H., Kurokawa, H., Mikami, B., and Hirose, M. (1999) Alternative structural state of transferrin. The crystallographic analysis of iron-loaded but domain-opened ovotransferrin N-lobe, *J. Biol. Chem. 274*, 10190−10194.
35. Donovan, J. W., Beardslee, R. A., and Ross, K. D. (1976) Formation of monoferric ovotransferrins in the presence of chelates, *Biochem. J. 153*, 631−639.
36. Faber, H. R., Bland, T., Day, C. L., Norris, G. E., Tweedie, J. W., and Baker, E. N. (1996) Altered domain closure and iron binding in transferrins: the crystal structure of the Asp60Ser mutant of the amino-terminal half-molecule of human lactoferrin, *J. Mol. Biol. 256*, 352−363.
37. Nicholson, H., Anderson, B. F., Bland, T., Shewry, S. C., Tweedie, J. W., and Baker, E. N. (1997) Mutagenesis of the histidine ligand in human lactoferrin: iron binding properties and crystal structure of the histidine-253→methionine mutant, *Biochemistry 36*, 341−346.
38. MacGillivray, R. T., Bewley, M. C., Smith, C. A., He, Q. Y., Mason, A. B., Woodworth, R. C., and Baker, E. N. (2000) Mutation of the iron ligand His 249 to Glu in the N-lobe of human transferrin abolishes the dilysine "trigger" but does not significantly affect iron release, *Biochemistry 39*, 1211−1216.
39. Baker, H. M., Mason, A. B., He, Q. Y., MacGillivray, R. T., and Baker, E. N. (2001) Ligand variation in the transferrin family: the crystal structure of the H249Q mutant of the human transferrin N-lobe as a model for iron binding in insect transferrins, *Biochemistry 40*, 11670−11675.
40. He, Q. Y., Mason, A. B., Woodworth, R. C., Tam, B. M., MacGillivray, R. T., Grady, J. K., and Chasteen, N. D. (1997) Inequivalence of the two tyrosine ligands in the N-lobe of human serum transferrin, *Biochemistry 36*, 14853−14860.
41. Khan, J. A., Kumar, P., Srinivasan, A., and Singh, T. P. (2001) Protein intermediate trapped by the simultaneous crystallization process. Crystal structure of an iron-saturated intermediate in the Fe^{3+} binding pathway of camel lactoferrin at 2.7 Å resolution, *J. Biol. Chem. 276*, 36817−36823.
42. Nagaoka, M. H., and Maitani, T. (2000) Differed preferential iron-binding lobe in human transferrin depending on the presence of bicarbonate detected by HPLC/high-resolution inductively coupled plasma mass spectrometry, *Biochim. Biophys. Acta 1523*, 182−188.
43. Ikeda, H., Nabuchi, Y., Nakazato, K., Tanaka, Y., and Satake, K. (1985) Preparation and characterization of trypsin-nicked ovotransferrin, *FEBS Lett. 182*, 305−309.
44. Oe, H., Doi, E., and Hirose, M. (1988) Amino-terminal and carboxyl-terminal half-molecules of ovotransferrin: preparation by a novel procedure and their interactions, *J. Biochem. (Tokyo) 103*, 1066−1072.
45. Williams, J., and Moreton, K. (1988) The dimerization of half-molecule fragments of transferrin, *Biochem. J. 251*, 849−855.

BI049147J